IEEE Access
Multidisciplinary ⋮ Rapid Review ⋮ Open Access Journal

Received 18 April 2023, accepted 19 May 2023, date of publication 27 June 2023, date of current version 6 July 2023.

Digital Object Identifier 10.1109/ACCESS.2023.3289843

RESEARCH ARTICLE

An Improvised Four-Port Multifunctional MIMO Antenna for Integrated Cognitive Radio System

PRANEET JAIN[1], (Student Member, IEEE), RAHUL KUMAR JAISWAL[2], (Student Member, IEEE), KUMAR VAIBHAV SRIVASTAVA[2], (Senior Member, IEEE), AND SAPTARSHI GHOSH[1], (Senior Member, IEEE)

[1]Department of Electrical Engineering, Indian Institute of Technology Indore, Indore, Madhya Pradesh 452020, India
[2]Department of Electrical Engineering, Indian Institute of Technology Kanpur, Kanpur, Uttar Pradesh 208016, India

Corresponding author: Saptarshi Ghosh (sghosh@iiti.ac.in)

This work was supported in part by Science and Engineering Research Board, India, under Project TTR/2021/000106.

ABSTRACT This article presents a four-port multiple input multiple output (MIMO) antenna designed and demonstrated for cognitive radio (CR) applications. The proposed geometry is made of a single-layer dielectric substrate, where metallic patterns and electronic components are articulately used to exhibit both types of CR techniques (interweave and underlay) through three different working states. In the first state, the antenna radiates over a wide bandwidth from 2.26 to 7.00 GHz for sensing applications, while in the second mode, the geometry has a frequency tunability between 4.80 to 6.20 GHz to be used for interweave CR communication. In the third mode, a fixed band-notch response is obtained at 4.20 GHz (which can also be made tunable from 3.10 to 4.80 GHz), thereby fulfilling the underlay operation. The novelties of the proposed work are the realization of an innovative antenna topology exhibiting all types of CR operations (102.38% in the wideband state, 14.4% in the tunable narrowband state, and 27.21% in the tunable bandnotch state), at the expense of using the lowest number of diodes components (2 p-i-n diodes and 1 varactor or 1 p-i-n diode and 2 varactors). Further, each of the design steps in the single antenna as well as MIMO geometry is in-depth analyzed by simulation, fabrication, and measurement responses.

INDEX TERMS Cognitive radio (CR) antenna, multiple input multiple output (MIMO), reconfigurable antenna, interweave antenna, underlay antenna.

I. INTRODUCTION

The information age of human civilization has propelled the use of wireless communication in the last few decades. It started with the development of wireless devices (mobile phone, Bluetooth, Wi-Fi, Wi-Max, near field communications, etc.) and the subsequent establishment of networks starting from 1st generation (1G) to all the way to 5G and beyond. Antennas have played a huge role in these developments and various protocols associated with them [1]. As the number of wireless device users is increasing exponentially, there is a need to utilize the spectrum efficiently and judiciously to accommodate future users, without compromising the speed and reliability of communication. This led to the introduction of the cognitive radio (CR) concept, where the system dynamically allocates specific parts of the spectrum to the users, based on their activities [2], [3], [4]. In CR, users are divided into two categories, namely primary users (PU) and secondary users (SU). Primary users are assigned to a fixed frequency spectrum, whereas secondary users are allowed to use the available spectrum unoccupied by the primary users [5], [6], [7], [8]. Two modes are generally used for efficient spectrum distribution between the users, viz. interweave mode and underlay mode [9], [10]. During the interweave mode, the CR device searches for the available frequency spectrum, commonly known as white space, and assigns it to the secondary users. In contrast, during the underlay mode of operation, the secondary users can co-exist

The associate editor coordinating the review of this manuscript and approving it for publication was Hassan Tariq Chattha.

with the primary users up to a specified level of interference. Fig. 1 presents interweave and underlay modes of operation graphically. In order to have the interweave mode, two types of antennas are desired: one is an ultra-wideband (UWB) channel sensing antenna and the other is a narrowband (NB) frequency reconfigurable antenna. The sensing antenna detects the white spaces in between the spectrum under-utilized by the primary users, whereas the tunable antenna regulates its operating frequency over those available spaces and allows the secondary users to communicate. During the underlay mode, the antenna should transmit UWB signals with a restricted power limit for simultaneous use of the spectrum among the users. But if the primary users require a higher level of isolation, the antenna should restrict the secondary users from transmitting in that frequency with a band stop characteristic. Thus, a UWB antenna with a notch band is desired for the secondary users in the underlay CR mode. Integration of both interweave and underlay operation into a single antenna device without compromising performance or reliability will be a significant advancement in wireless communication. The requirement for high-speed data transmission along with better reliability has made the multiple input multiple output (MIMO) antenna systems one of the indispensable parts of modern-day wireless communications, in particular, aiming at 5G and future mobile networks [11], [12], [13], [14]. MIMO antennas with the capability to support CR can greatly improve spectrum utilization along with maintaining data security and integrity. However, designing an antenna system with both MIMO and CR characteristics on a single substrate is a challenging task. CR concept involves the use of reconfigurable elements, such as p-i-n diodes, varactors, and their associated biasing circuits [15], [16]. Although other types of switching/ tuning elements can be used in CR operation [17], [18], [19], electronically reconfigurable elements have various advantages, like compact size, low cost, robustness, and commercial availability. On the contrary, MIMO antennas with diverse characteristics are reported over a wide frequency range, starting from sub-6 GHz to the Terahertz range [20]. Different mechanisms, such as electromagnetic bandgap, defected ground structure, metamaterial, etc. have been explored to attain various responses, like- high isolation [21], [22], [23], wide bandwidth [24], large gain [25], and/or circularly polarization behaviour [26]. Over the last few years, various design techniques are reported presenting MIMO and CR concepts in single or separate devices. Ref. [27] presents a 2-port antenna structure exhibiting the UWB response at 2.6 to 12 GHz and NB around 5.8 GHz, aiming for the interweave mode of operation. A number of p-i-n diodes are used in a Vivaldi antenna to offer multiple states of operation across a wide bandwidth in Ref. [28]. In Refs. [29] and [30], varactor diodes are introduced to exhibit a UWB/tunable NB operation. However, all the above geometries are single element based topologies (without any MIMO configuration) and limited to interweave mode of operation only. In Ref. [31], a 2-port MIMO antenna switching between wideband (from 3.4 to 8.0 GHz) and narrowband (from 4.7 to 5.4 GHz) responses is presented with polarization diversity characteristic. A multi-band frequency reconfigurable MIMO antenna system is demonstrated in Ref. [32], which covers a wideband operation from 0.70 to 3.66 GHz under one mode and exhibits multiple narrowband frequencies between 0.75 and 3.45 GHz under the other mode. The tunability in the narrowband operation has been achieved in Ref. [33] by loading a varactor diode to cover a frequency range from 1.77 to 2.51 GHz, while the UWB mode is attained in the range of 0.75 to 7.65 GHz. But the antenna geometries exhibit interweave type of CR responses only. Tawk et. al. has designed two separate MIMO antennas in Ref. [34], where one geometry can be used for the interweave operation (showing switchable broadband/tunable narrowband response), and the other geometry can be used for the underlay mode (presenting two notch band responses, one of which is reconfigurable). Recently, both interweave and underlay CR operations are integrated into single antenna structures, where p-i-n diodes and varactors are mounted across different positions exhibiting multiple operations [35], [36], [37]. However, the topologies utilize a large number of electronic components (6 set of p-i-n diodes and varactors in each antenna element), thereby having higher design complexity and parasitic effects. The use of such a large number of components has further increased the biasing circuit intricacy as well as led to several unused logic levels (61 states). In addition, the performances of the antennas need to be improved with respect to critical parameters (impedance bandwidth, operating gain, tuning range, etc.) in the CR system. Therefore, designing a MIMO system with a minimal number of electronic components while exhibiting all types of CR modes (interweave and underlay) as well as maintaining satisfactory antenna performances is exceptionally challenging but highly desired.

This paper presents a 4-port MIMO antenna functioning for both interweave and underlay modes by utilizing only two p-in diodes and one varactor (for each element). The antenna design consists of a modified ellipsoidal patch at the end of a feed line in the top layer and a defected ground structure (DGS) at the bottom layer of a dielectric. By careful regulation of the diode elements, all three working states, viz. a UWB response, a tunable NB response, and a band notch (BN) response are realized satisfying both the modes of CR operation. The UWB state can be operated ranging from 2.26 to 7.00 GHz (with a fractional bandwidth of 102.4%), the NB state has a frequency tunability between 4.50 and 5.20 GHz, and the notch band is observed at 4.20 GHz under the third state. While realizing the four-port MIMO antenna, a thin metallic strip is inserted between the face-to-face elements to attain the desired isolation. The other MIMO antenna parameters are all under acceptable limits. Each of the design steps, starting from the single passive antenna to the final multifunctional MIMO antenna, has been analyzed with full-wave simulation and measurement results. The similarity between the responses validate the proposed

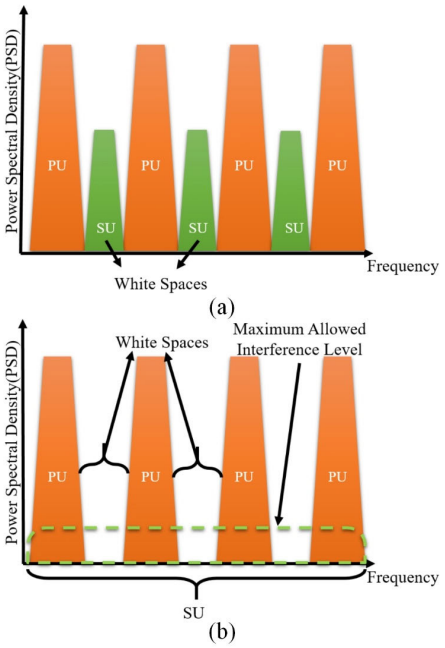

FIGURE 1. Cognitive radio techniques: (a) interweave mode, (b) underlay mode.

concepts, while discussions are provided to justify small deviations, if any.

The primary novelty of our proposed work is the realization of an innovative technique by positioning the three separate uncorrelated segments (UWB geometry, NB geometry, and BN geometry) very close to each other in a multifunctional antenna structure to achieve both CR operations (interweave and underlay). This subsequently leads to the use of a minimal number of lumped components (3 diodes in each antenna) which results in a simpler biasing circuit and reduced antenna complexity (the number of unused logic levels is decreased from 61 to 5). In addition, several performance parameters of the MIMO antenna (like impedance bandwidth, operating gain, etc.) are considerably improved with respect to the referred articles.

The rest of the paper is organized as follows. Section II discusses the single-element passive antenna and its switchable counterpart. Section III incorporates other reconfigurable properties into the switchable antenna, thus presenting a multifunctional antenna. Fabricated prototypes and their measured responses are also described in corresponding sections. Thereafter, the MIMO antenna configuration and its performance are illustrated in Section IV, along with its measured parameters. Finally, the discussion is presented in Section V, followed by the conclusive remarks in Section VI.

II. SINGLE ELEMENT ANTENNA

The final multifunctional MIMO antenna design has been conceptualized from a single element passive antenna geometry and subsequently evolved through various steps.

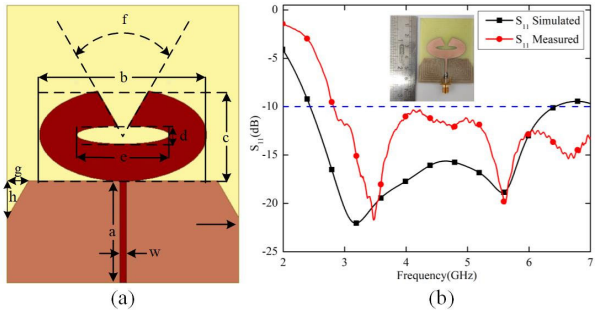

FIGURE 2. (a) Proposed single element passive antenna geometry, and (b) comparison between simulated and measured reflection coefficient. Inset shows the photograph of the antenna prototype.

The details of each stage and their corresponding responses are discussed in the below subsections.

A. SINGLE ELEMENT PASSIVE ANTENNA

The passive antenna is designed on a single layer dielectric substrate, whose top metallic pattern is made of an ellipsoidal patch fed by a microstrip line and the bottom layer is a defected ground plane [38]. An FR4 substrate relative permittivity (ε_r) of 4.4 and dielectric loss tangent ($tan\,\delta$) of 0.02 is used as the constituent dielectric with a thickness of 0.8 mm. The overall dimensions of the antenna geometry are 50 mm $\times$ 60 mm. Other geometrical parameters are mentioned as follows: a = 22 mm, b = 36 mm, c = 20 mm, d = 4 mm, e = 20 mm, $f = 35°$, $g = 4.6$ mm, w = 1.4 mm, and $h = 8$ mm. The topology is depicted in Fig. 2(a). The antenna structure, owing to its ellipsoidal topology, exhibits a UWB response from 2.40 GHz to 6.00 GHz with the reflection coefficient (S_{11}) amplitude lying below -10 dB value. The geometry provides an average gain above 4.5 dBi across the operating bandwidth with a maximum gain of 6.0 dBi in the broadside direction at 5.60 GHz. The passive antenna has been fabricated using the printed circuit board (PCB) technique. The reflection coefficient of the prototype is measured and plotted against the simulated response, as shown in Fig. 2(b). A wideband characteristic is obtained ranging from 2.80 GHz to 7.00 GHz, thus having a reasonable agreement with the simulated result. The fabricated antenna is also shown in the inset of the figure.

B. SINGLE ELEMENT SWITCHABLE ANTENNA

To incorporate the switchable activity in the passive antenna design without disturbing the UWB characteristic, a p-i-n diode is mounted across the microstrip feed line and a metallic sidearm is added to the existing topology. BAP 70-03 from NXP semiconductors is used as the p-i-n diode in the geometry, with an ON state resistance of 1.5 ohm and an OFF state capacitance of 1.5 pF [39]. A lumped capacitor with a value of 0.1 pF is also inserted across the top gap of the sidearm. The switchable antenna geometry is depicted in Fig. 3(a) and the parameters highlighted in the figure have the following values: $i = 0.8$ mm, $j = 10.4$ mm, and

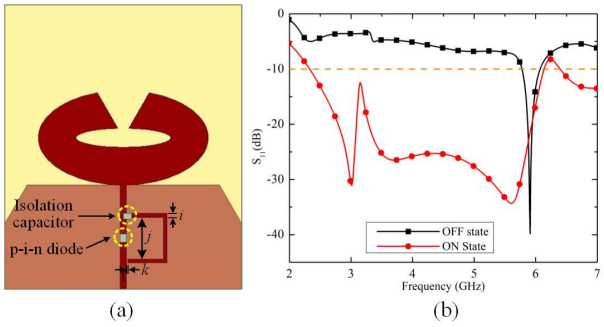

FIGURE 3. (a) Proposed single element switchable antenna geometry, and (b) its simulated reflection coefficient response under different biasing states.

k = 0.3 mm. The remaining dimensions are the same as that of the passive geometry. To design a switchable antenna from the existing passive antenna design, modifications are made with minimal design alteration and the addition of a single diode component. When the diode is under the forward bias, it offers a small resistance and the incident signal flows through the original feed line towards the ellipsoidal patch, thereby retaining its UWB response. In contrast, during the reverse bias, the diode exhibits a large capacitance that drives the electromagnetic (EM) wave to flow through the sidearm. The sidearm metallic length along with its associated gap presents a distributed series *LC* circuit and allows the signal to pass at a particular frequency. This causes the ellipsoidal patch to radiate at that frequency only, and an NB response is realized during the OFF state of the diode. The simulated S_{11} response for both ON and OFF states of the switchable antenna is shown in Fig. 3(b). During the OFF state, the NB response is obtained at 5.90 GHz, whereas the UWB response is retained between 2.35 and 6.00 GHz under ON state. The UWB state can be used as the sensing antenna, whereas the NB state can be utilized to assign the spectrum to the secondary users under the interweave mode of operation. To explain the design mechanism, the antenna topology is illustrated for three different cases in Fig. 4, viz. Case 1: geometry without any gap in the sidearm, Case 2: geometry with a gap in the sidearm but no capacitor mounted, and Case 3: geometry with a lumped capacitor mounted across the top gap in the sidearm. When no gap is exerted in the sidearm geometry (Case 1), the incident signal receives a continuous metal path irrespective of the diode conditions (ON or OFF state), and NB responses are obtained in both states. A decoupling technique in the sidearm is thus necessary to obtain the UWB response during the ON state of the diode. A small gap of 0.3 mm (=k) is provided at both ends of the sidearm in this regard (Case 2). However, this degrades the NB response under the OFF state. To retain both the NB and UWB properties, a lumped capacitor has been added across the top gap in the sidearm geometry (Case 3), which provides a good isolation during ON state of the diode but assists in coupling the sidearm with the microstrip when the diode is off.

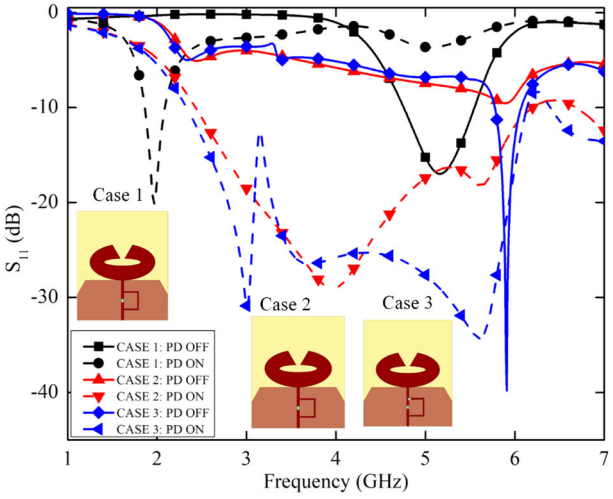

FIGURE 4. S_{11} responses of the single element switchable antenna for different stages; Case 1: without any gap in sidearm, Case 2: with a gap in sidearm but no capacitor, and Case 3: with a capacitor across the gap in sidearm.

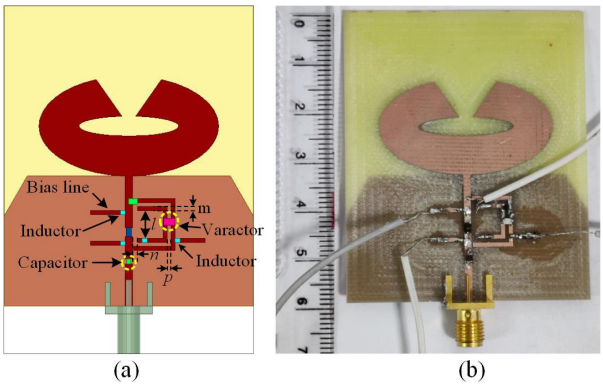

FIGURE 5. (a) Proposed single element antenna with switchable and tunable characteristics, and (b) photograph of fabricated prototype.

TABLE 1. Summary of the working states.

Lower p-i-n diode (PD1)	Upper p-i-n diode (PD2)/ Varactor diode (VD2)	Varactor diode (VD1)	Responses	CR Operations
ON	PD2/ VD2: ON	Idle	UWB	Interweave
OFF	PD2/ VD2: ON	Tunable	Tunable NB	Interweave
ON	PD2: OFF	Idle	Fixed BN	Underlay
ON	VD2: Tunable	Idle	Tunable BN	Underlay

C. SINGLE ELEMENT TUNABLE AND SWITCHABLE ANTENNA

Once the switching response is achieved, the next step is to realize the tunable NB response for operating the antenna in the interweave mode. One varactor diode is introduced along with an additional side arm in the existing switchable geometry, as depicted in Fig. 5(a). SMV1249 varactor diode

TABLE 2. Comparison table.

References	No. of states (UWB, NB, BN)	Bandwidth under different states; Gain (UWB: Ultra wideband, NB: Narrowband, BN: Band notch)			No. of p-i-n diodes	No. of varactors
		UWB	NB	BN		
[30]	2 (UWB, NB)	3.40 – 8.00 GHz; 4.00 dBi	5.3-5.7 GHz (Switchable); 4.0 dBi	-	6	0
[31]	2 (UWB, NB)	0.71 – 3.60 GHz; 4.00 dBi	0.75-3.45 GHz (Switchable); 4.0 dBi	-	2	0
[32]	2 (UWB, NB)	0.75 – 7.65 GHz; 5.30 dBi	1.77-2.51 GHz (Tunable); 1.5-3.0 dBi	-	0	1
[33]	2 (UWB, NB)	3.00 – 6.00 GHz; N.A.	4.00 – 4.50 GHz (Switchable); N.A.	-	4	0
	1 (BN)	-	-	3.60 GHz (Fixed); N.A.	1	0
[35]	3 (UWB, NB, BN)	1.60 – 4.50 GHz (95.08%); 1-3 dBi	2.80 – 3.65 GHz (Tunable); 1-3 dBi	2.60 – 3.30 GHz (Tunable); 1-3 dBi	5	1
[36]	3 (UWB, NB, BN)	2.45 – 5.30 GHz (73.55%); N.A.	3.60 – 4.20 GHz (Tunable); N.A.	3.10 – 3.85 GHz (Tunable); N.A.	3	3
[37]	3 (UWB, NB, BN)	2.50 – 5.60 GHz (76.54%); 4.0 dBi	3.20 – 4.30 GHz (Tunable); 4.0 dBi	3.10 – 4.50 GHz (Tunable); 4.0 dBi	5	1
This work	**3 (UWB, NB, BN)**	**2.26 – 7.00 GHz (102.38%); 2.50 dBi**	**4.80 – 6.20 GHz (Tunable); 1.30-2.20 dBi**	**4.20 GHz (Fixed); 2.10 dBi**	**2**	**1**
				3.10 – 4.80 GHz (Tunable); 2.10 dBi	**1**	**2**

from Skyworks has been used in the geometry that provides a wide range of junction capacitance from 2.03 to 37.35 pF while varying the reverse bias voltage [40]. The physical dimensions of the additional sidearm geometry are mentioned as follows: $l = 7.1$ mm, $m = 0.8$ mm, $n = 1$ mm, and $p = 0.8$ mm, whereas the remaining structure is similar to the above switchable antenna. The proposed antenna has two sets of diodes; one is a p-i-n diode (which is mounted across the central feed) and the other is a varactor diode (which is embedded between two sidearm geometries). When the p-i-n diode is under the forward bias, the incident signal directly flows towards the ellipsoidal patch, resulting in a UWB response from 2.47 GHz to 6.20 GHz (with S_{11} below -10 dB). The varactor diode is kept idle at this case. During the reverse bias condition of the p-i-n diode, the signal flows through the sidearm geometry and the NB response is resulted at 5.80 GHz. The design concept is similar to the switchable antenna discussed above, except for a slight shift in the operating frequency owing to the addition of the second sidearm. Under this NB state (i.e., when the p-i-n diode is OFF), the signal passes through the varactor, and by changing the reverse voltage, its junction capacitance can be varied, thereby tuning the NB response over a wide operating range. The varactor diode may also be placed along the length of any of the sidearm geometries, but in that case, the varactor capacitance would appear in series with that of the gap capacitance present at each end of the sidearm. This gap capacitance, being distributed in nature, has a very small value (in the order of fF) and would bring down the overall capacitance of the sidearm (because of their series combination). This would severely reduce the tuning range under the interweave operation. However, with the proposed configuration, the varactor capacitance appears in parallel with that of the gap capacitance and marks its prominent effect in the NB response in attaining a wide tuning range [41], [42]. The antenna geometry is thereafter fabricated and the lumped components are mounted across different gaps. Direct current (DC) bias circuits are also designed to provide the biasing voltages across the diodes, without disturbing the EM response. Two narrow-width metal lines are drawn on the left side of the central feed to provide the DC voltage across the p-i-n diode. Each line is equipped with one lumped inductor to block the radio frequency (RF) signal from the voltage source. In a similar way, two points (along with inductors) are created at the right side of the sidearm geometry for providing the biasing voltage across the varactor diode. A lumped capacitor is also mounted near the end of the feed line to block the DC from the RF source. The inductor and capacitor values are chosen such that they cover the entire operating range. The fabricated antenna prototype along with the mounted components is depicted in Fig. 5(b). While increasing the revere bias voltage across the varactor diode, the junction capacitance value reduces, and consequently the NB response tunes over a wide frequency range. The full wave simulation result is presented in Fig. 6 and a 1 GHz wide tuning range, starting from 4.30 to 5.30 GHz, is observed while varying the capacitance value between 37 to 2.5 pF (which is the available range for SMV 1249-079 varactor). Owing to some difficulty in arranging the varactor diode, the responses were measured by placing different values of lumped capacitors in the place of the varactor while matching with its junction capacitance value. The measured and simulated reflection coefficient responses are plotted in Fig. 6 and they are observed to be in good agreement. Thus, the interweave operation has been achieved with this designed antenna.

III. SINGLE ELEMENT MULTIFUNCTIONAL ANTENNA

A. DESIGN AND ANALYSIS

The antenna design presented in the above section has the capability of exhibiting a UWB response (under the ON state of the p-i-n diode and idle condition of the varactor), and a tunable NB response (under the OFF state of the p-i-n diode and different bias voltages across the varactor).

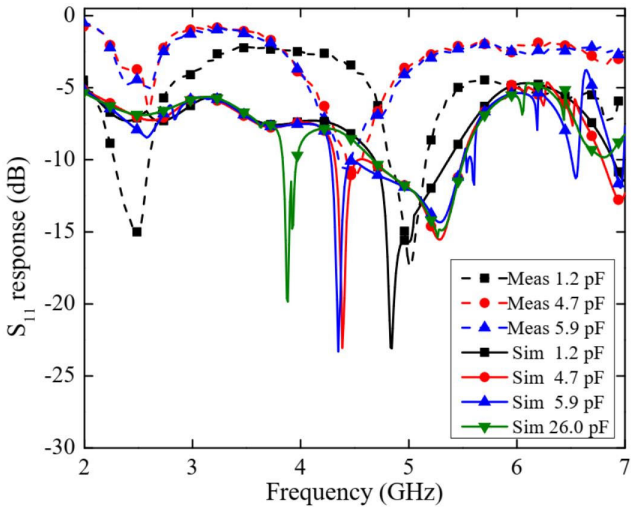

FIGURE 6. Comparison of measured and simulated S_{11} response of the single element antenna under NB state (p-i-n diode: OFF, varactor diode: varying).

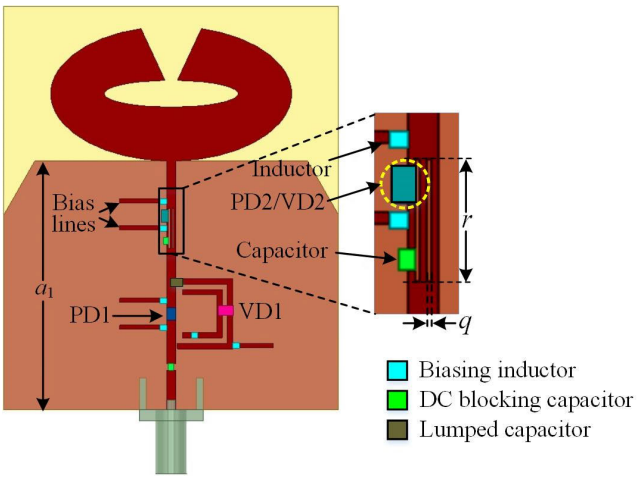

FIGURE 7. Proposed single element multifunctional antenna geometry.

However, to implement the proposed geometry in full-scale CR applications (i.e., operating for both interweave and underlay modes), one BN characteristic has to be incorporated into the existing design. For realizing a notched band inside a UWB response, the incoming signal needs to be blocked at a particular frequency, whereas the EM wave at other frequencies should be allowed towards the ellipsoidal patch. A modification is made accordingly to design the final antenna structure, offering all such characteristics. Fig. 7 shows the single element multifunctional antenna geometry, where two parallel slot lines are introduced in the central feed along with one p-i-n diode (PD2) mounted across the gap in the left strip. To accommodate the set of slot lines, the feed line length is increased with respect to the previous design. Other dimensions remain constant as before. The values of the parameters modified/ newly added in this topology are as follows: $a_1 = 37$ mm, $r = 6$ mm, and $q = 0.25$ mm. The p-i-n diode (PD1) and varactor (VD1) used in the previous section are kept similar as before. Each of the p-i-n diode is modeled as an ON state resistance of 1.5 ohm and an OFF state capacitance of 1.5 pF. The varactor is replaced with a tunable capacitor ranging between 1.2 pF and 37.35 pF.

When the p-i-n diodes (PD1 and PD2) are under forward bias, all the strip lines assist in reaching the incident signal to the ellipsoidal patch, thereby retaining the UWB response as before. But, when the diode PD2 is under reverse bias, the OFF state capacitance, along with the distributed inductance generated by the strip lines, offers a BN response amidst the UWB characteristic. The PD1 is biased under forward state and the bias voltage across the varactor diode is kept idle. The switchable BN state can also be made tunable by replacing the PD2 with a varactor diode (VD2), as marked in Fig. 7. By regulating the reverse voltage across this varactor, the notch band can be tuned over a wide frequency. The biasing circuit designed for PD2 can also be used for VD2, and the response can be attained without any difficulty. The same varactor under forward bias exhibits a small resistance and the overall response will get switched to the UWB mode, thus replicating the PD2 switch performance.

While generating the notch band response with the above condition, the other two working states remain almost unaffected owing to the difference in their working principles. Thus, with the use of only three switches (either PD1-VD1-PD2 combination or PD1-VD1-VD2 combination), three different functions required for the full-scale CR application can be accomplished. The operations are summarized in Table 1.

An equivalent circuit model along with its schematic diagram of the proposed multifunctional antenna are presented in Figs. 8(a) and 8(b), respectively. The structure is made of three closely positioned segments (UWB geometry, NB geometry, and BN geometry) uncorrelated with one another. By careful regulation of the diode elements, the current can be selectively passed through either one or two segments, and the particular mode of operation can be achieved accordingly. When both PD1 and PD2 are under forward bias, the electrical current flows through the diode elements owing to their low resistance paths (R_{PD1} and R_{PD2}) and reaches the ellipsoidal patch, thereby contributing to the UWB mode of operation. No other capacitance is encountered in the path except for the DC blocking capacitors (C_1 and C_3), as depicted in Fig. 8(c). When PD1 is reverse biased and PD2 is forward biased, the current flows through the side path containing the varactor diode (VD1) and the PD2 element. Then the junction capacitance of VD1 (C_{VD1}) can be tuned by varying the reverse bias voltage, which in turn results in a tunable NB response. The inductance and capacitance (L_2, C_2, and C_4) associated with this side path assist in attaining the NB characteristic, as shown in Fig. 8(d). Finally, when PD1 is forward biased and PD2 is reverse biased, the OFF state capacitance of PD2 (C_{PD2}), along with the distributed inductance generated by the strip lines (L_3), offers the BN response. An alternative circuit replacing the PD2 with a varactor diode (VD2) results in a tunable BN state,

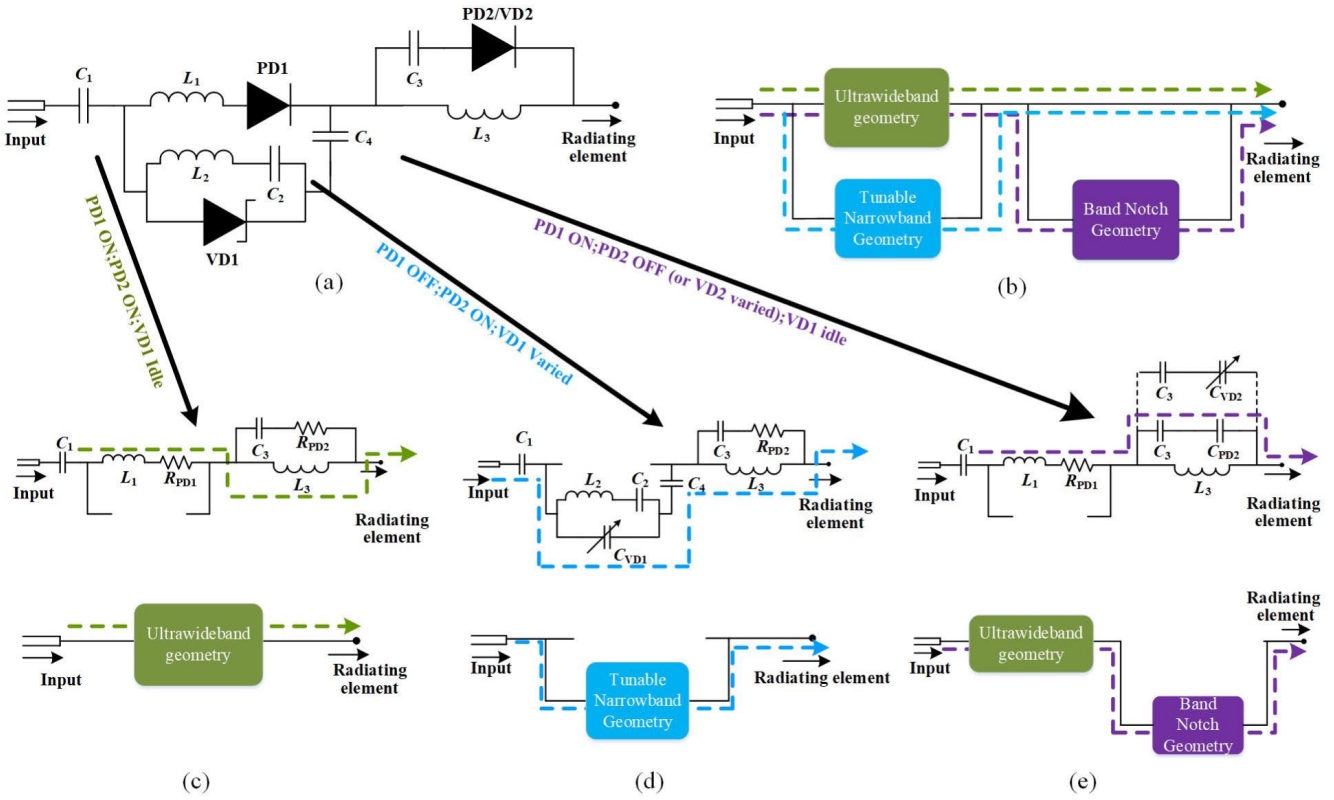

FIGURE 8. (a) Equivalent circuit depicting the operation mechanism of the proposed multifunctional antenna, and (b) schematic diagram for controlling various operational states in the geometry, (c) UWB state of operation, (d) narrowband state of operation and (e) bandnotch response state of operation.

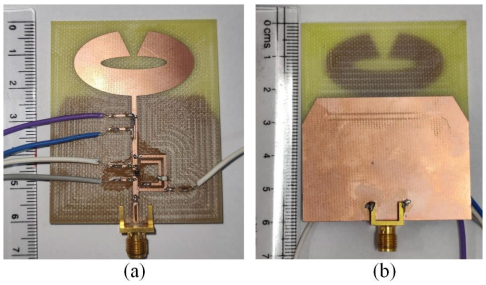

FIGURE 9. Photograph of the fabricated antenna: (a) top view, (b) bottom view.

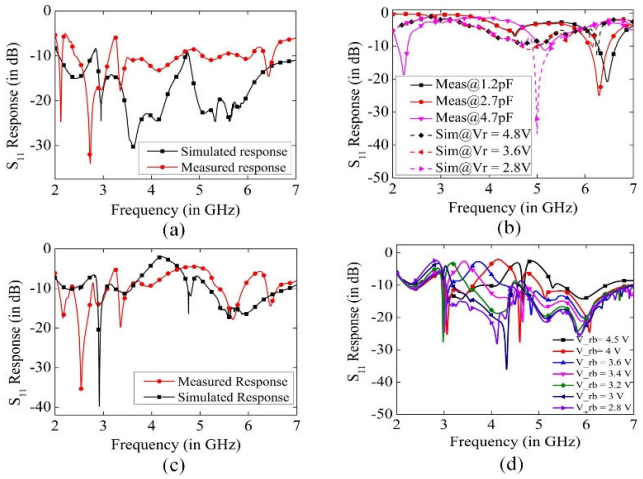

FIGURE 10. S_{11} responses. (a) UWB state for sensing operation, (b) tunable NB state for interweave mode, (c) fixed band notch state for underlay mode, and (d) simulated tunable band notch response for complete underlay operation.

while varying the junction capacitance (C_{VD2}) using the bias voltage. Fig. 8(e) describes this underlay mode of operation. The bias line inductances are ignored in the circuit model for simplicity, and the DC blocking capacitors are chosen such that they will not participate in any resonance.

B. SIMULATED AND MEASURED RESPONSE

To validate the design concept, the proposed antenna geometry is simulated along with the requisite biasing lines. The RF signal and DC voltage are isolated with the help of DC blocking lumped capacitors C_1 and C_3 (of 4.7 nH) and bias line inductors (of 7.5 nH) at appropriate locations. The single element multifunctional antenna is then fabricated on an FR4 substrate of 0.8 mm thickness and the lumped components (PD1, PD2, VD1, inductors, capacitors) are soldered using surface mount technique. Fig. 9 depicts the photograph of the fabricated prototype. Both the measured and simulated responses for all three working states are demonstrated. Under the UWB state, as shown in Fig. 10(a), the simulated geometry exhibits a wide bandwidth from 2.26 to 7.0 GHz (except for two small glitches appearing

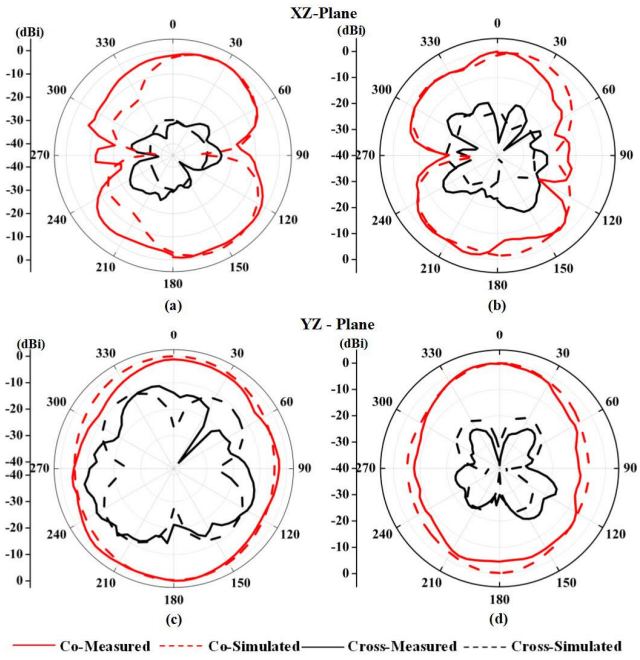

FIGURE 11. Simulated and measured radiation patterns for single antenna under UWB mode of operation: (a) XZ plane at 3.27 GHz, (b) XZ plane at 5.38 GHz, (c) YZ plane at 3.27 GHz, and (d) YZ plane at 5.38 GHz.

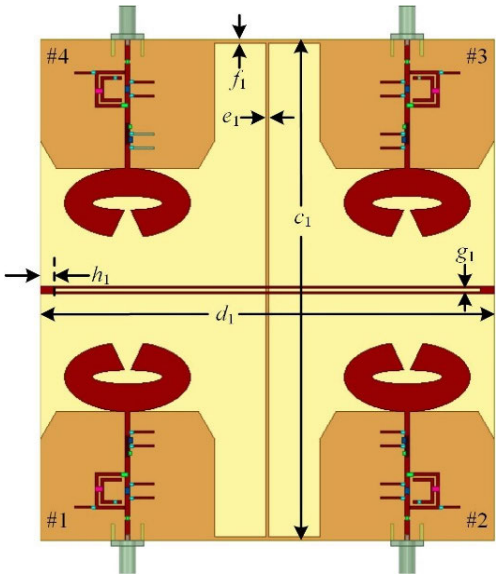

FIGURE 12. Proposed multifunctional MIMO antenna geometry.

around 3.25 and 5.0 GHz), whereas the measured response is more uniform in nature having a coverage from 2.4 GHz to 6.8 GHz. The second state, as depicted in Fig. 10(b), offers a tunable narrowband response ranging from 4.80 GHz to 6.20 GHz. The prototype, while measured with different valued capacitors, offers a similar tuning range although a bit shifted in the high frequency. Fig. 10(c) illustrates the underlay operation, where a stop band bandwidth of 1.6 GHz (from 3.6 GHz to 5.2 GHz) is achieved inside a wideband operation (from 2.92 GHz to 6.83 GHz). The

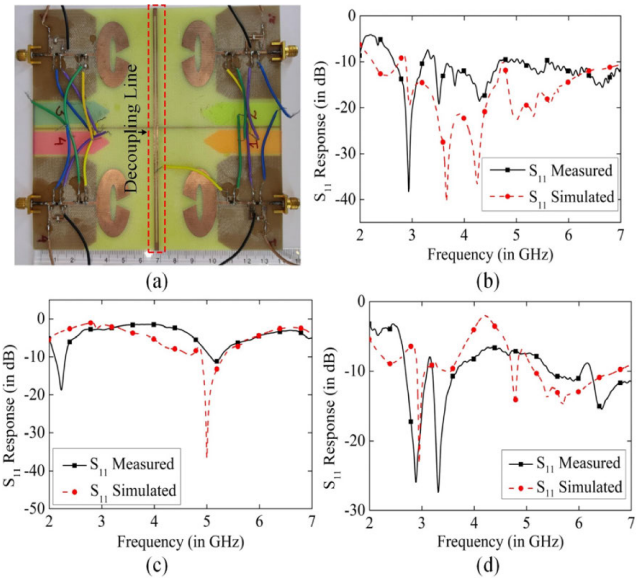

FIGURE 13. (a) Fabricated antenna geometry. Comparison of simulated and measured S_{11} responses of the proposed MIMO antenna: (b) UWB state, (c) NB state, and (d) band notch state.

measured result also shows a similar BN characteristic around 5 GHz. The geometry is fabricated with the PD1-VD1-PD2 combination, whereas the other combination PD1-VD1-VD2 is demonstrated in full-wave simulation. Fig. 10(d) presents the simulated tunable notch band response ranging from 3.10 to 4.80 GHz, while replacing PD2 with VD2. The measured responses resemble the simulated plots in all the cases along with some minor deviations, which can be attributed to the fabrication tolerance, parasitic values of the lumped components, and small interference from the biasing wires.

The radiation pattern of the proposed antenna is plotted at two different frequencies, viz. 3.27 GHz and 5.38 GHz for one of the operating states (UWB condition) in Fig. 11. The patterns depict slightly titled broadside radiation with a cross polarization level of less than -15 dB at both frequencies. The gain of the antenna is measured inside an anechoic chamber using a standard procedure [43], [44], and is observed to be around 2.5 dBi. The efficiency has been calculated under the UWB mode and found to be slightly reduced to 84% (in case of the multifunctional antenna) from 95% (in case of the passive antenna). The measured efficiency is at par with the simulated efficiency under UWB operation [44] and can be validated for other cases as well.

IV. MULTIFUNCTIONAL MIMO ANTENNA

Once the single-element antenna is designed, the geometry has been extended to four ports, resulting in the MIMO antenna. While replicating the antenna elements in the MIMO configuration, a slotted metal line is printed on the top side to improve the isolation between face-to-face antennas (1st and 4th, 2nd and 3rd). The design exhibits a parallel *LC* resonance and reduces the interference by reflecting the unwanted

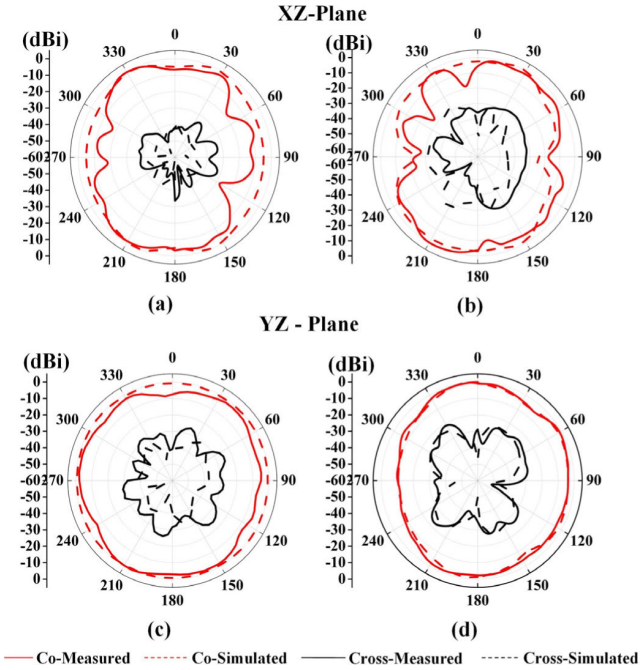

FIGURE 14. Simulated and measured radiation pattern of the proposed MIMO antenna for UWB state: for XZ plane at (a) 4.42 GHz, and (b) 5.32 GHz; for YZ plane at (c) 4.42 GHz, and (d) 5.32 GHz.

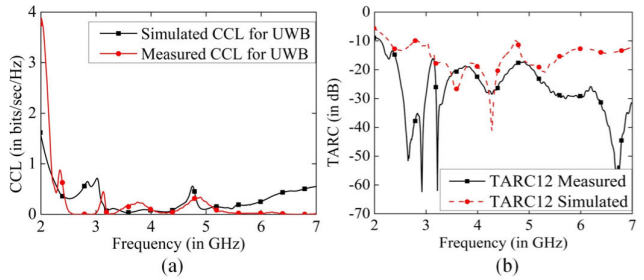

FIGURE 15. Comparison of simulated and measured response of the proposed MIMO antenna for UWB state: (a) CCL plot, and (b) TARC plot.

radiation from end fire direction. Thin metal strips are used to connect the ground planes together. Fig. 12 depicts the proposed geometry along with dimensions inscribed inside the figure. The values are as follows: $c_1 = 144$ mm, $d_1 = 130$ mm, $e_1 = 1$ mm, $f_1 = 1$ mm, $g_1 = 2.4$ mm, and $h_1 = 4$ mm.

The design is then studied in Ansys HFSS as well as fabricated using PCB technique. Fig. 13(a) illustrates the photograph of the MIMO structure, indicating the decoupled line and other key segments. Both the simulated and measured responses for all three states are plotted in Figs. 13(b)-(d) to demonstrate the proposed concept in the MIMO system. The UWB state exhibits a wide bandwidth from 2.26 to 7.00 GHz, the NB state exhibits an interweave operation around 4.85 GHz (for single capacitor value), and a stop bandwidth of 1.6 GHz (from 3.6 to 5.2 GHz) is obtained under underlay mode. In all cases, the measured responses follow the simulated patterns. The radiation patterns for the MIMO antenna are also plotted at two frequencies 4.42 and

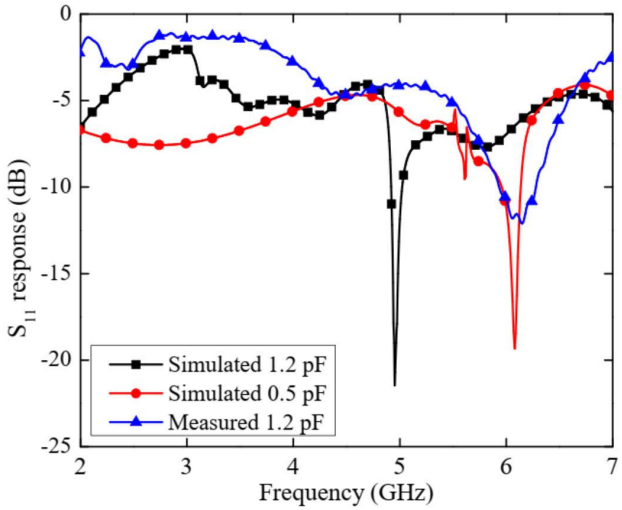

FIGURE 16. Comparison of simulated and measured response of the proposed multifunctional antenna geometry (discussed in Section III) under different capacitance values.

5.32 GHz for UWB condition in Fig. 14. The patterns depict likewise responses to the single antenna element, where the primary radiation is towards the broadside direction with a slight tilt and a cross-polarization level is less than -15 dB. The peak gain is found to be around 2.50 dBi with an 80% efficiency. Afterward, several MIMO antenna parameters are studied for evaluating the performance of the geometry. The envelope correlation coefficient (ECC) of the first antenna is determined with respect to other antennas from scattering parameters [43], and the value is well below than the accepted value of 0.5, as depicted in Fig. 15(a). The channel capacity loss (CCL) is also determined and is found to lie below 0.5 bits/sec/Hz across the entire operating bandwidth. The total active reflection coefficient (TARC) has also been determined for the UWB state and both the simulated and measured responses appear below −10 dB level, as depicted in Fig. 15(b).

V. DISCUSSION

While measuring the antenna geometries for different working states, a deviation in the operating frequency is observed between the simulated and measured results. Although the shift is limited in case of the UWB and BN states, there is a noticeable deviation observed for the NB state in different antenna structures designed above. The possible reasons behind such a difference can be attributed to the fabrication tolerance, bias network effects, and/or measurement inaccuracy, but above all, the lumped components are the primary source of error in the response. The component used in the varactor diode position seems to have a larger tolerance limit as well as offers an unwanted inductance at high frequency. Moreover, the technical datasheets of the diodes and other lumped components used in the design are available till a few hundreds of MHz, whereas the frequencies of operation of the proposed antenna structure are up to 7 GHz. Since the actual

parasitic values at this high frequency couldn't be determined, the given datasheet values were used in full wave simulation. It is highly likely that the actual values of the components get deviated with frequencies and cause these shifts in the S-parameters.

As a proof of concept, the multifunctional antenna geometry (discussed in Section III) is studied with different capacitor values in the place of the varactor (VD1), and the measured NB state response with a 1.2 pF capacitor is found to have a close agreement with that of the simulated response corresponding to a 0.5 pF capacitor, as depicted in Fig. 16. A frequency deviation of around 1 GHz is observed between the simulated and measured values for 1.2 pF capacitor, which perfectly aligns with the difference observed in the antenna geometries. For other lumped components (p-i-n diodes, inductors) used in the structure, either the tolerance limits are small or parasitic element values are negligible, thereby causing minor deviation between the simulated and measured responses across other operating states.

VI. CONCLUSION

A four-port MIMO antenna is presented exhibiting all three working states (UWB, NB, and bandstop) for different CR techniques (interweave and underlay). The design focuses on the utilization of a minimum number of diode components (2 p-i-n diodes and 1 varactor or 1 p-i-n diode and 2 varactors) for attaining all three operations as well as exhibits largest bandwidths under different states (102.4% under UWB and 14.4% under NB), as evident from Table 2. The proposed concept has been investigated in a detailed procedure, starting from the single element passive antenna, switchable antenna, switchable and tunable antenna, multifunctional antenna, and lastly the multifunctional MIMO antenna, while each step has been analyzed with simulation, fabrication, and measurement responses. Both the antenna geometries and biasing circuits are simple yet innovative in nature and can further be expanded for a higher number of ports in the MIMO topology. Thus, the proposed MIMO antenna can be deployed for CR applications in various wireless devices aimed at 5G communication.

REFERENCES

[1] C. A. Balanis, *Antenna Theory: Analysis and Design*. 4th ed. New York, NY, USA: Wiley, 2016.
[2] Y. Tawk, J. Costantine, and C. G. Christodoulou, "Cognitive-radio and antenna functionalities: A tutorial [wireless corner]," *IEEE Antennas Propag. Mag.*, vol. 56, no. 1, pp. 231–243, Feb. 2014.
[3] J. Mitola, "Cognitive radio architecture evolution," *Proc. IEEE*, vol. 97, no. 4, pp. 626–641, Apr. 2009.
[4] X. Zhao, S. Riaz, and S. Geng, "A reconfigurable MIMO/UWB MIMO antenna for cognitive radio applications," *IEEE Access*, vol. 7, pp. 46739–46747, 2019.
[5] J. Mitola and G. Q. Maguire, "Cognitive radio: Making software radios more personal," *IEEE Pers. Commun.*, vol. 6, no. 4, pp. 13–18, Aug. 1999.
[6] J. Mitola, "Cognitive radio: An integrated agent architecture for software-defined radio," Ph.D. dissertation, Royal Inst. Technol. (KTH), Stockholm, Sweden, 2000.
[7] S. Haykin, "Cognitive radio: Brain-empowered wireless communications," *IEEE J. Sel. Areas Commun.*, vol. 23, no. 2, pp. 201–220, Feb. 2005.
[8] O. P. Awe, A. Deligiannis, and S. Lambotharan, "Spatio-temporal spectrum sensing in cognitive radio networks using beamformer-aided SVM algorithms," *IEEE Access*, vol. 6, pp. 25377–25388, 2018.
[9] A. Goldsmith, S. A. Jafar, I. Maric, and S. Srinivasa, "Breaking spectrum gridlock with cognitive radios: An information theoretic perspective," *Proc. IEEE*, vol. 97, no. 5, pp. 894–914, May 2009.
[10] Y. Tawk, S. K. Jayaweera, C. G. Christodoulou, and J. Costantine, "A comparison between different cognitive radio antenna systems," in *Proc. Int. Symp. Intell. Signal Process. Commun. Syst. (ISPACS)*, Dec. 2011, pp. 1–5.
[11] S. Chen and J. Zhao, "The requirements, challenges, and technologies for 5G of terrestrial mobile telecommunication," *IEEE Commun. Mag.*, vol. 52, no. 5, pp. 36–43, May 2014.
[12] T. S. Rappaport, S. Sun, R. Mayzus, H. Zhao, Y. Azar, K. Wang, G. N. Wong, J. K. Schulz, M. Samimi, and F. Gutierrez, "Millimeter wave mobile communications for 5G cellular: It will work!" *IEEE Access*, vol. 1, pp. 335–349, 2013.
[13] (May 2022). *IEEE 5G and Beyond Technology Roadmap White Paper*. [Online]. Available: https://futurenetworks.ieee.org/images/files/pdf/-ieee-5g-roadmap-white-paper.pdf
[14] Y. Niu, Y. Li, D. Jin, L. Su, and A. V. Vasilakos, "A survey of millimeter wave communications (mmWave) for 5G: Opportunities and challenges," *Wireless Netw.*, vol. 21, no. 8, pp. 2657–2676, Apr. 2015.
[15] R. Hussain and M. S. Sharawi, "A cognitive radio reconfigurable MIMO and sensing antenna system," *IEEE Antennas Wireless Propag. Lett.*, vol. 14, pp. 257–260, 2015.
[16] G. Srivastava, A. Mohan, and A. Chakrabarty, "Compact reconfigurable UWB slot antenna for cognitive radio applications," *IEEE Antennas Wireless Propag. Lett.*, vol. 16, pp. 1139–1142, 2017.
[17] Y. Tawk and C. G. Christodoulou, "A new reconfigurable antenna design for cognitive radio applications," *IEEE Antennas Wireless Propag. Lett.*, vol. 8, pp. 1378–1381, 2009.
[18] Y. Tawk, J. Costantine, K. Avery, and C. G. Christodoulou, "Implementation of a cognitive radio front-end using rotatable controlled reconfigurable antennas," *IEEE Trans. Antennas Propag.*, vol. 59, no. 5, pp. 1773–1778, May 2011.
[19] G. P. Jin, D. L. Zhang, and R. L. Li, "Optically controlled reconfigurable antenna for cognitive radio applications," *IET Electron. Lett.*, vol. 47, no. 17, pp. 948–950, Aug. 2011.
[20] M. S. Sharawi, *Printed MIMO Antenna Engineering*. Norwood, MA, USA: Artech House, 2014.
[21] T. K. Roshna, U. Deepak, V. R. Sajitha, K. Vasudevan, and P. Mohanan, "A compact UWB MIMO antenna with reflector to enhance isolation," *IEEE Trans. Antennas Propag.*, vol. 63, no. 4, pp. 1873–1877, Apr. 2015.
[22] C. Luo, J. Hong, and L. Zhong, "Isolation enhancement of a very compact UWB-MIMO slot antenna with two defected ground structures," *IEEE Antennas Wireless Propag. Lett.*, vol. 14, pp. 1766–1769, 2015.
[23] M. Naser-Moghadasi, R. Ahmadian, Z. Mansouri, F. B. Zarrabi, and M. Rahimi, "Compact EBG structures for reduction of mutual coupling in patch antenna MIMO arrays," *Prog. Electromagn. Res. C*, vol. 53, pp. 145–154, 2014.
[24] D. Sarkar and K. V. Srivastava, "A compact four-element MIMO/diversity antenna with enhanced bandwidth," *IEEE Antennas Wireless Propag. Lett.*, vol. 16, pp. 2469–2472, 2017.
[25] A. A. Ibrahim and W. A. E. Ali, "High gain, wideband and low mutual coupling AMC-based millimeter wave MIMO antenna for 5G NR networks," *AEU-Int. J. Electron. Commun.*, vol. 142, Dec. 2021, Art. no. 153990.
[26] N. Hussain, M. Jeong, A. Abbas, and N. Kim, "Metasurface-based single-layer wideband circularly polarized MIMO antenna for 5G millimeter-wave systems," *IEEE Access*, vol. 8, pp. 130293–130304, 2020.
[27] I. Messaoudene, T. A. Denidni, and A. Benghalia, "Experimental investigations of ultra-wideband antenna integrated with dielectric resonator antenna for cognitive radio applications," *Prog. Electromagn. Res. C*, vol. 45, pp. 33–42, 2013.
[28] M. R. Hamid, P. Gardner, P. S. Hall, and F. Ghanem, "Switched-band Vivaldi antenna," *IEEE Trans. Antennas Propag.*, vol. 59, no. 5, pp. 1472–1480, May 2011.
[29] E. Erfani, J. Nourinia, C. Ghobadi, M. Niroo-Jazi, and T. A. Denidni, "Design and implementation of an integrated UWB/reconfigurable-slot antenna for cognitive radio applications," *IEEE Antennas Wireless Propag. Lett.*, vol. 11, pp. 77–80, 2012.

[30] S. Koley, D. Bepari, and D. Mitra, "Band-reconfigurable monopole antenna for cognitive radio applications," *IETE J. Res.*, vol. 61, no. 4, pp. 411–416, Jul. 2015.
[31] B. P. Chacko, G. Augustin, and T. A. Denidni, "Electronically reconfigurable uniplanar antenna with polarization diversity for cognitive radio applications," *IEEE Antennas Wireless Propag. Lett.*, vol. 14, pp. 213–216, 2015.
[32] R. Hussain and M. S. Sharawi, "Integrated reconfigurable multiple-input-multiple-output antenna system with an ultra-wideband sensing antenna for cognitive radio platforms," *IET Microw., Antennas Propag.*, vol. 9, no. 9, pp. 940–947, Jun. 2015.
[33] R. Hussain, M. S. Sharawi, and A. Shamim, "An integrated four-element slot-based MIMO and a UWB sensing antenna system for CR platforms," *IEEE Trans. Antennas Propag.*, vol. 66, no. 2, pp. 978–983, Feb. 2018.
[34] Y. Tawk, J. Costantine, and C. G. Christodoulou, "Reconfigurable filtennas and MIMO in cognitive radio applications," *IEEE Trans. Antennas Propag.*, vol. 62, no. 3, pp. 1074–1083, Mar. 2014.
[35] S. R. Thummaluru, M. Ameen, and R. K. Chaudhary, "Four-port MIMO cognitive radio system for midband 5G applications," *IEEE Trans. Antennas Propag.*, vol. 67, no. 8, pp. 5634–5645, Aug. 2019.
[36] T. Alam, S. R. Thummaluru, and R. K. Chaudhary, "Improved multifunctional MIMO cognitive radio system for integrated interweave-underlay operations," *IEEE Trans. Microw. Theory Techn.*, vol. 70, no. 1, pp. 631–640, Jan. 2022.
[37] K. Tyagi, A. K. Dwivedi, S. K. Singh, P. Ranjan, and A. Sharma, "Four port dielectric resonator based MIMO antenna design for cognitive radio applications," *IEEE Trans. Circuits Syst. II, Exp. Briefs*, vol. 70, no. 6, pp. 1936–1940, Jun. 2022.
[38] P. Jain and S. Ghosh, "A reconfigurable four-port MIMO antenna for sub-6 GHz applications," in *Proc. IEEE Wireless Antenna Microw. Symp. (WAMS)*, Jun. 2022, pp. 1–5.
[39] (May 2022). *BAP70-03 Datasheet*. [Online]. Available: https://www.nxp.com/docs/en/data-sheet/BAP70-03.pdf
[40] (May 2022). *Skywork SMV 1249 Datasheet*. [Online]. Available: https://www.skyworksinc.com/Products/Diodes/SMV1249-Series
[41] S. Ghosh and K. V. Srivastava, "Polarisation-independent tunable absorber with embedded biasing network," *Electron. Lett.*, vol. 53, no. 17, pp. 1176–1178, Aug. 2017.
[42] S. Ghosh and K. V. Srivastava, "Broadband polarization-insensitive tunable frequency selective surface for wideband shielding," *IEEE Trans. Electromagn. Compat.*, vol. 60, no. 1, pp. 166–172, Feb. 2018.
[43] L. H. Hemming, *Electromagnetic Anechoic Chambers: A fundamental Design and Specification Guide*. Hoboken, NJ, USA: Wiley, 2002.
[44] Z. N. Chen, D. Liu, H. Nakano, X. Qing, and T. Zwick, *Handbook of Antenna Technologies*. Singapore: Springer, 2016.
[45] M. S. Sharawi, "Printed multi-band MIMO antenna systems and their performance metrics [wireless corner]," *IEEE Antennas Propag. Mag.*, vol. 55, no. 5, pp. 218–232, Oct. 2013.

PRANEET JAIN (Student Member, IEEE) was born in Bhopal, India, in 1998. He received the B.E. degree in electronics and communication engineering from the R. V. College of Engineering, India, in 2020. He is currently pursuing the M.S. degree in electrical engineering (research) with the Indian Institute of Technology Indore, India. His current research interests include reconfigurable microwave antennas for cognitive radio, reconfigurable antennas, and 3D printed conformal antenna.

RAHUL KUMAR JAISWAL (Student Member, IEEE) received the B.Tech. degree in electronics and communication engineering from Uttar Pradesh Technical University, Lucknow, India, in 2012, and the M.Tech. degree in microwave electronics from the University of Delhi South Campus, Delhi, India, in 2016. He is currently pursuing the Ph.D. degree in RF and microwaves discipline with the Electrical Engineering Department, Indian Institute of Technology Kanpur, India, under the supervision of Prof. Kumar Vaibhav Srivastava. He worked as a Project Trainee with the Society for Applied Microwave Electronics Engineering and Research (SAMEER), Kolkata, from 2015 to 2016. He was a Scientist with the Institute for Plasma Research (IPR), Gandhinagar, India, from 2016 to 2017. He has published several journals/conference papers on various aspects of antennas and RF waveguides. His research interests include MIMO antennas, circularly polarized antennas, unidirectional and bidirectional end-fire CP antennas, base station antennas, and full-duplex antennas. He received the IEEE Antennas and Propagation Society Doctoral Research Grant, in 2021. Currently, he is serving as the Chair for IEEE APS-SBC at IIT Kanpur, India.

KUMAR VAIBHAV SRIVASTAVA (Senior Member, IEEE) received the B.Tech. degree in electronics engineering from the Kamla Nehru Institute of Technology, Sultanpur, India, in 2002, and the M.Tech. and Ph.D. degrees in electrical engineering from the Indian Institute of Technology Kanpur, Kanpur, India, in 2004 and 2008, respectively. He was with the GE Global Research Centre, Bengaluru, India, in 2008. In 2009, he joined as an Assistant Professor with the Department of Electrical Engineering, IIT Kanpur, where he has been a Professor, since November 2018. He has published more than 115 international journal articles, two international patents, and 150 conference papers, in the last 15 years. His research interests include microwave antennas, metamaterials, metamaterial absorbers and cloaking, FDTD technique, and MIMO Antennas. He received various national and best paper awards. He was the Chairperson of the IEEE UP Section, in 2018, and the founding Chair of the IEEE Antenna and Propagation Society Chapter in the UP Section.

SAPTARSHI GHOSH (Senior Member, IEEE) received the B.E. degree in electronics and telecommunication engineering from IIEST, Shibpur, India, in 2009, and the M.Tech. and Ph.D. degrees in electrical engineering from the Indian Institute of Technology Kanpur, Kanpur, India, in 2013 and 2017, respectively.

He was with Chung-Ang University, Seoul, South Korea, as a Postdoctoral Researcher, for one year, and joined the Department of Electrical Engineering, Indian Institute of Technology Indore, India, where he is currently an Assistant Professor, since December 2018. He has authored or coauthored more than 50 international journal articles and 70 conference papers during his research career. His current research interests include metamaterials, microwave absorbers, frequency-selective surfaces, and millimeter-wave antennas.

Dr. Ghosh received the Young Engineer Award from INAE, in 2022; the IETE-IRSI (83) Young Scientist Award from IETE, in 2022; the Motohisa Kanda Award from IEEE EMC Society, in 2022; the Young Scientist Award from URSI, in 2022 and 2018; the MIF Fellowship from Japan, in 2020; the Young Innovative Student Projects Award from INAE, in 2018; and several best paper awards, in 2022, 2018, 2017, 2016, and 2013. He has also received outstanding reviewer awards from IEEE TRANSACTIONS ON ANTENNAS AND PROPAGATION and IEEE ANTENNAS AND WIRELESS PROPAGATION LETTERS, from 2021 to 2019. He has been serving as an Associate Editor for IEEE ANTENNAS AND WIRELESS PROPAGATION LETTERS, since 2021.